Physicochem. Probl. Miner. Process., 60(3), 2024, 189908

http://www.journalssystem.com/ppmp

Physicochemical Problems of Mineral Processing

ISSN 1643-1049

Insight into the mechanism on co-leaching of REEs and Fe from NdFeB sludge: Elucidating phase transformation and co-leaching kinetics

Xinglan Li [1,2], Zishuai Liu [1,2], Xiu Liu [3], Xuekun Tang [1,2], Huiyang Lin [1,2], Lushuai Yao [1,2], Wanting Bai [1,2], Jiangfeng Guo [1,2]

[1] Jiangxi Provincial Key Laboratory of Environmental Pollution Prevention and Control in Mining and Metallurgy, Jiangxi University of Science and Technology, Ganzhou 341000, China

[2] Key Laboratory of Testing and Tracing of Rare Earth Products for State Market Regulation, Jiangxi University of Science and Technology, Ganzhou 341000, China

[3] Chinalco Environmental Protection and Energy Conservation Group Co., Ltd., Beijing 101300, China

Corresponding authors: liuzishuai87@126.com (Zishuai Liu), liuyu335@163.com (Xiu Liu)

Abstract: The NdFeB sludge is a secondary rare earth resource abundant in both REEs and Fe elements. However, there tends to be a focus on recovering only high-value rare earths while neglecting the recycling of high-content iron, leading to a low comprehensive utilization of this secondary rare earth resource. The present study builds upon previous research on the separation and coextraction of REEs and Fe from NdFeB sludge, further investigating the phase transformation behavior during oxidation roasting and elucidating the kinetics of simultaneous leaching of REEs and Fe. The results suggest that NdFeB waste exhibited a loose morphology and demonstrated high susceptibility to dissolution in hydrochloric acid when subjected to roasting temperatures below 500℃. The morphology of NdFeB waste becomes denser and more spherical, hindering its dissolution in hydrochloric acid when the roasting temperature exceeded 500℃, resulting in a reduction in the leaching efficiencies of both roasting. The co-leaching of REEs and Fe in NdFeB sludge is governed by internal diffusion for REEs and chemical reaction for Fe, as evidenced by the kinetic results. Furthermore, it is observed that the apparent activation energy of rare earth surpasses that of iron, leading to the attainment of equilibrium for rare earth prior to that of iron during the synchronous leaching process. The findings of this study hold theoretical significance in enhancing the overall efficiency of secondary rare earth resource utilization.

Keywords: NdFeB sludge, rare earth, iron, phase transformation, co-leaching kinetics

1. Introduction

The NdFeB is a rare earth magnetic material renowned for its exceptional performance, extensively utilized in the domains of electronics, electric machinery, aerospace, medical equipment, hardware machinery, and other related industries (Prosperi et al., 2018; Ambaye et al., 2020). The processing procedure of NdFeB involves the stages of melting, hydrogenation, shaping, sintering, and processing. During the processing, a significant amount of NdFeB sludge is generated as a result of grinding, cutting, and other manufacturing processes (Brião et al., 2022; Jyothi et al., 2020). These sludges contain approximately 20-30% rare earth elements (REEs) and 60-70% iron (Fe), rendering them highly valuable from an economic standpoint (Jyothi et al., 2020; Chen et al., 2023). The direct disposal of the sludge would result in significant waste of rare earth metals and iron resources. The recovery of valuable metals, such as REEs and Fe, from this kind of waste is of significant importance for the recycling and sustainable development of secondary rare earth resources.

The recycling of NdFeB waste has been extensively investigated in recent years, encompassing methods such as hydrochloric acid preferential dissolution, complete dissolution extraction, electrochemistry, and microwave-assisted techniques (Venkatesan and sun et al., 2018; Venkatesan and Hoogerstraete et al., 2018; Awais et al., 2020; Behera and Parhi, 2019; Kumari et al., 2021). Among them,

DOI: 10.37190/ppmp/189908

the hydrochloric acid preferential dissolution method was the most widely employed technique for production and application (Du et al., 2023). Its primary principle involved oxidizing and roasting NdFeB sludge at temperatures ranging from 700℃, to 900℃, followed by the addition of an appropriate quantity of hydrochloric acid to selectively dissolve the chemically more reactive oxidized rare earths ((Du et al., 2023; Belfqueh et al., 2023). Meanwhile, a small amount of chemically less reactive oxidized Fe may or may not be dissolved, thereby achieving targeted leaching of REEs. The leachate obtained through the hydrochloric acid preferential dissolution method was subsequently supplemented with an extraction agent, enabling targeted separation and enrichment of REEs by adjusting the pH of the solution. Alternatively, the leachate can be neutralized and purified before being treated with oxalate or carbonate to precipitate the rare earths, thereby facilitating their recovery (Yang et al., 2024; Yu et al., 2024). The recycling and utilization of valuable rare earth resources have been facilitated by many researchers who have selectively extracted rare earths from various NdFeB sludge (Brião et al., 2024; He et al., 2022).

Although the recovery of rare earths from NdFeB sludge has been extensively researched and the production process was well-established, researchers tended to prioritize the extraction of high-value REEs due to their significant price disparity with iron. Consequently, they often overlooked the potential for recovering iron resources with higher content, resulting in a suboptimal comprehensive utilization rate of secondary rare earth resources. Therefore, the recycling process of NdFeB sludge will result in the generation of a significant quantity of solid waste containing iron once again, thereby impeding the sustainable development of the rare earth industry (Jin et al., 2018). To this end, we proposed a process to separate and co-extract REEs and Fe from NdFeB sludge by co-leaching and stepwise precipitation (Liu et al., 2022). Through the low-temperature oxidative roasting and hydrochloric acid leaching of NdFeB sludge, REEs and Fe were co-leached, followed by precipitation of rare earth using oxalic acid and reduction precipitation of iron. This comprehensive recovery approach yields REES in the form of $RE_2(C_2O_4)_3 \cdot 10H_2O$ while obtaining Fe as $FeC_2O_4 \cdot H_2O$ (Liu et al., 2022). However, our research has found that during the roasting process of NdFeB sludge, there were significant variations in the phase transformation of REEs and Fe, and the leaching rates of the two during the co-leaching process were also significantly different. Simultaneously, the focus on preferential dissolution of REEs after high-temperature oxidation roasting of NdFeB sludge has overshadowed the phase transformation process during iron oxidation roasting, leading to uncertainties regarding the phase transformate behavior of REEs and Fe in the roasting process as well as an incomplete understanding of the dissolution mechanism during co-leaching processes involving REEs and Fe. Although extensive scholarly research has been conducted on the leaching kinetics of selective recovery of REEs from NdFeB sludge (Kumari et al., 2018; Behera et al., 2016), the current studies primarily focused on the selective leaching process of rare earths and overlook the disparity in leaching rates between rare earths and iron during this process.

In this paper, the phase transformation and co-leaching kinetics of REEs and Fe from NdFeB sludge was investigated based on our previous research findings. The phase transformation of REEs and Fe in the oxidation roasting process of NdFeB sludge was investigated using XRD and SEM techniques, aiming to discern the dissimilarities in dissolution between REEs and Fe in the NdFeB sludge after oxidation roasting. By investigating the co-leaching kinetics of REEs and Fe to discern the disparity in leaching rates between these two elements, thereby elucidating the dissolution mechanism underlying their leaching process.

2. Experimental

2.1. Materials and reagents

NdFeB sludge samples were obtained from a rare earth recycling company situated in Ganzhou, Jiangxi province, China. The NdFeB sludge was subjected to a detergent wash at 60°C for 60 minutes, followed by filtration. These steps were repeated three times consecutively. Subsequently, the deoiled NdFeB waste, containing a minimal amount of oil, underwent roasting at 400°C for 120 minutes to obtain the experimental NdFeB waste. The chemical composition of the NdFeB waste is listed in Table 1. The research showed that the iron and rare earth content of the sample is 50.28% and 25.65%, respectively.

Table 1. Chemical components of NdFeB sample (%)

Element	Nd	Gd	Pr	Ce	Fe	Al	Mg	Ca	Si
Content	10.85	7.81	5.62	1.37	50.28	1.83	0.05	0.16	0.28

2.2. Experimental operations

Roasting experiments: Conducted roasting experiments by introducing a suitable quantity of purified NdFeB sample into a crucible, followed by transferring the crucible to a muffle furnace set at specific temperature and duration for oxidative roasting, aiming to obtain NdFeB roasted clinker. Finally, ground the clinker to achieve a particle size of -0.074mm, ensuring complete utilization for leaching and characterization purposes.

Leaching experiments: Leaching experiments were conducted by introducing the roasted NdFeB sample and hydrochloric acid into a beaker, followed by stirring and leaching at a specified temperature and duration with a rotational speed of 500 r/min. After completion of the reaction, a solid-liquid separation process was carried out to obtain the leachate and residue, which were subsequently subjected to comprehensive analysis and characterization. The leaching efficiencies of REEs and Fe were determined using the following formula:

$$\mathrm{E} = \frac{\mathrm{CV}}{\beta \mathrm{m}} \times 100\% \quad (1)$$

where E represents the leaching efficiency of metal ions, expressed as a percentage (%); C denotes the concentration of metal ions in the leachate, measured in grams per liter (g/L); V indicates the volume of the leachate, measured in liters (L); β represents the grade of metal in NdFeB, expressed as a percentage (%); and m signifies the mass of NdFeB waste.

2.3. Analytical methods

The concentrations and grades of REEs in the NdFeB and leachate were analyzed using single channel scan inductively coupled plasma emission spectroscopy (ICP, ULTIMA 2, JOBIN YVON, France), respectively. Take 0.2 grams of dried NdFeB waste and place it in a 250-mL conical flask. Subsequently, add 30 mL of hydrochloric acid with a 50% volume concentration and 10 mL of nitric acid with a 50% volume concentration, respectively. Heat the mixture thoroughly on an electric heating plate, maintaining a temperature of 200 °C for a duration of 30 minutes. Once all solid components are dissolved, allow the solution to cool, then dilute and adjust the volume to 100 mL in a volumetric flask. Lastly, procure a sample of the diluted solution for the ICP detection.

The levels of total Fe in the NdFeB waste and leachate were determined using potassium dichromate titration, assessing both grades and concentrations (Standardization Administration of the People's Republic of China, 2009). The grades and concentrations of the other impurity ions in the NdFeB waste and leachate were determined using inductively coupled plasma emission spectroscopy (ICP-OES, IRIS Intrepid II, Thermo Electron Corporation, USA), respectively. The phase compositions were identified by X-ray diffraction (XRD, D8 Advance, Bruker, Germany). Microscopic observations were conducted by using field emission scanning electron microscopy (SEM, ΣIGMA, Carl Zeiss, Germany).

3. Results and discussion

3.1. Phase transformation of REEs and Fe during oxidizing roasting

3.1.1. Effect of roasting temperature

The NdFeB magnets are composed of REEs and Fe, both of which occur in metallic form. The direct acid leaching of NdFeB waste generated a significant amount of hydrogen, which poses safety concerns and hinders the production process. Therefore, in the production process, NdFeB waste was typically subjected to oxidation roasting followed by hydrochloric acid leaching. To investigate the phase transformation behavior of REEs and Fe during the oxidation roasting process, we examined the impact of different roasting temperatures on the leaching efficiencies of REEs and Fe. The conditions for the co-leaching of REEs and Fe were determined as follows: a hydrochloric acid concentration of 6 mol/L,

liquid-solid ratio of 5:1, leaching temperature of 90°C, and leaching time of 120 min. The results are shown in Fig. 1.

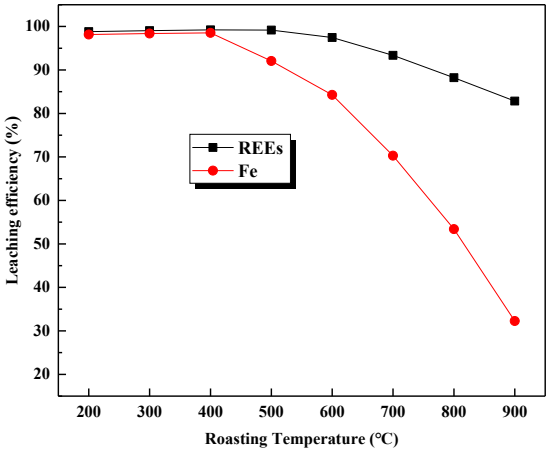

Fig. 1. Effect of roasting temperature on the leaching efficiencies of REEs and Fe

The leaching efficiencies of REEs and Fe exhibited a decreasing trend with increasing roasting temperature, as illustrated in Fig. 1. The leaching efficiency for the REEs remained consistently high and approached 100% throughout a roasting temperature range of 200-500 °C. The leaching efficiency of REEs exhibited a gradual decline, ranging from 99.16% to 82.84%, with an increase in the roasting temperature from 500 °C to 900 °C. The leaching efficiency of Fe showed minimal variation when the roasting temperature ranged from 200 to 400 °C. The leaching efficiency of Fe significantly decreased from 98.52% to 32.27% with an increase in the roasting temperature from 400 °C to 900 °C.

According to previous studies, the roasting of NdFeB waste was identified as an oxidation reaction process, with the corresponding reaction equations presented as follows:

$$4RE + 3O_2 = 2RE_2O_3 \quad (1)$$

$$4Fe + 3O_2 = 2Fe_2O_3 \quad (2)$$

Interestingly, despite the elevated temperature conditions, complete oxidation of REEs and Fe was not achieved as evidenced by the significant decrease in leaching efficiencies, indicating that certain fractions of REEs and Fe remained insoluble to hydrochloric acid. The roasted products and leached residues obtained at different temperatures were subjected to XRD analysis in order to determine the cause of the decrease in REEs and Fe leaching efficiency. The results are shown in Fig. 2.

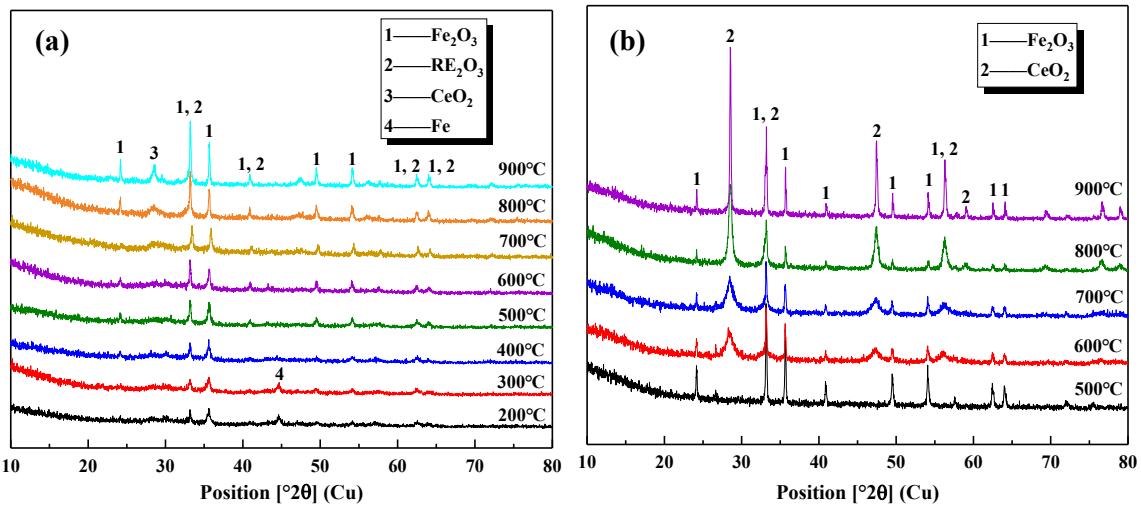

Fig. 2. XRD pattern of the roasted products (a) and leached residues (b) under different roasting temperature

As shown in Fig. 2(a), the roasted products showed different phases at different roasting temperatures. All the roasted products mainly existed in the form of Fe_2O_3 and RE_2O_3. The appearance of the Fe phase was observed in the roasted product when the roasting temperature reached 200 °C and 300 °C. The Fe phase vanished when the roasting temperature surpassed 400 °C. The observation indicates that incomplete oxidation of iron occurs during low temperature roasting, resulting in the presence of residual metallic iron in the roasted products. The complete oxidation of REEs and Fe was achieved when the temperature was raised above 400 °C. When the roasting temperature reached 200 °C and 300 °C, a significant amount of bubbles were observed during the leaching test. This phenomenon can be attributed to the abundant generation of hydrogen resulting from the dissolution of metallic iron in hydrochloric acid. The production of a significant quantity of hydrogen during the leaching process, however, contradicts safety protocols in place for production. When the roasting temperature reached 400 °C, minimal bubbling was observed during the leaching process. Therefore, the roasting temperature of 400 °C was chosen based on the comparable leaching efficiencies of REEs and Fe within the range of 200~500 °C.

The roasting temperature exceeded 400 °C, resulting in almost complete oxidation of REEs and Fe; however, this led to a significant reduction in the leaching efficiencies of both REEs and Fe. It noteworthy that the presence of the CeO_2 phase was observed in the roasted products when the roasting temperature exceeded 600 °C. The low solubility of CeO_2 in acid may account for the decrease in leaching efficiency of REEs. As depicted in Fig. 2(b), Fe was predominantly present as Fe_2O_3, while REEs were primarily present as CeO_2 in the leaching residue at temperatures ranging from 500 to 900 °C. The dissolution of Nd, Pr, Gd, and other rare earth oxides is nearly complete, whereas CeO_2 exhibits incomplete dissolution. The decrease in leaching efficiency of REEs with increasing roasting temperature can be attributed to the formation of insoluble CeO_2 during high-temperature roasting, as evidenced by this observation. In addition, when the roasting temperature exceeds the optimal range, acid-soluble phases such as $NdFeO_3$ and $GdFeO_3$ are formed due to the reaction between rare earth and iron, leading to a reduction in the leaching rate of rare earth elements (Firdaus et al, 2018; Zhang et al, 2022). The reason behind the decrease in Fe leaching efficiency, however, remains unexplained. In order to determine the causes behind the decrease in Fe leaching efficiency, SEM analysis was conducted on both the roasted products and leached residues. The results are shown in Fig. 3 and Fig. 4.

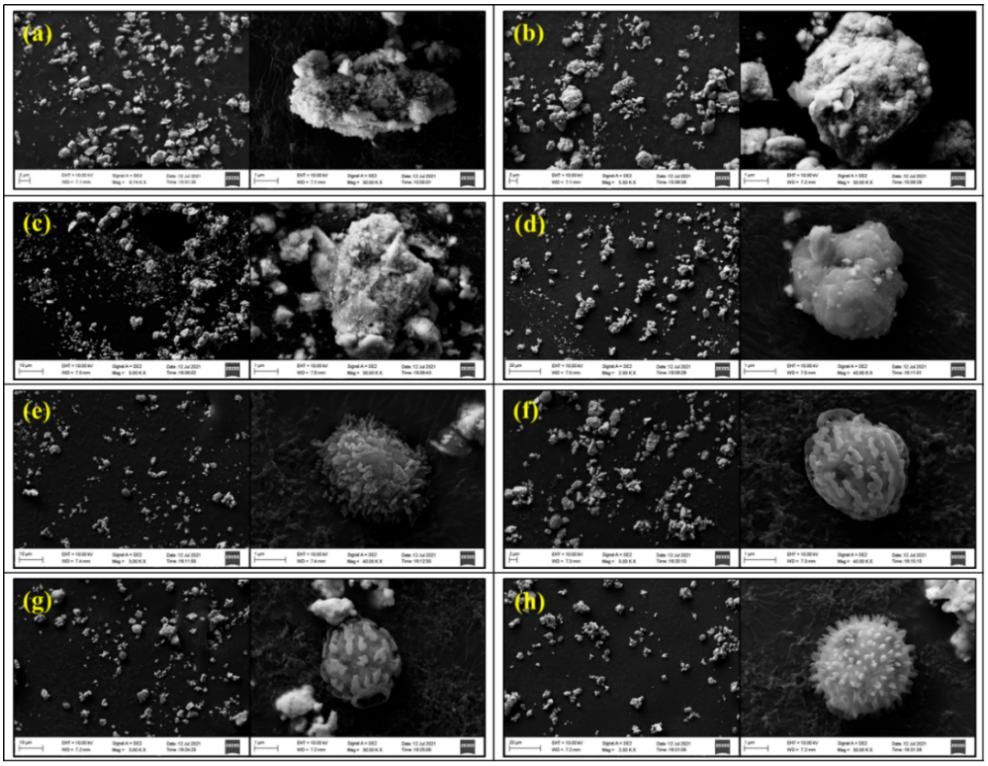

(a) 200 °C; (b) 300 °C; (c) 400 °C; (d) 500 °C; (e) 600 °C; (f) 700 °C; (g) 800 °C; (h) 900 °C

Fig. 3. SEM of the roasted products under different roasting temperature

The morphology of the roasted products exhibited a porous structure, as depicted in Fig. 3, indicating that hydrochloric acid could easily permeate into the core of NdFeB waste through its loose surface when the roasting temperature was below 400 ℃. The presence of RE_2O_3 and Fe_2O_3 in NdFeB waste was effectively identified. The morphology of NdFeB waste transformed into a smooth and dense structure when the roasting temperature reached 500℃. By further increasing the roasting temperature, a compact "walnut" spherical structure was observed in the NdFeB waste. Additionally, as depicted in Fig. 4, when the roasting temperature surpassed 500℃, the morphology of the leaching residue continued to exhibit a compact "walnut" spherical structure, thereby indicating an exceptional resistance to dissolution of said "walnut" spherical structure. The decrease in Fe leaching efficiency with increasing roasting temperature can be attributed to the following reason: At high roasting temperatures, the NdFeB waste undergoes sintering and forms a compact walnut-like structure, making it difficult for hydrochloric acid to penetrate into the structure and resulting in incomplete dissolution of Fe_2O_3.

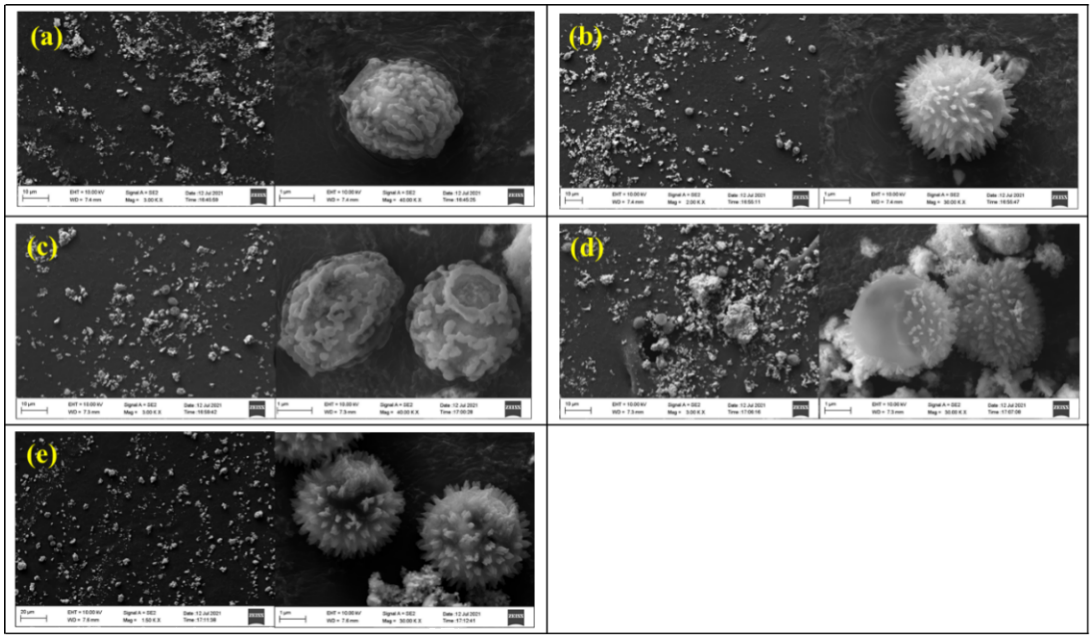

(a) 500 °C; (b) 600 °C; (c) 700 °C; (d) 800 °C; (e) 900 °C

Fig. 4. SEM of the leaching residues under different roasting temperature

3.1.2. Effect of roasting time

The phase transformation behavior of REEs and Fe during oxidation roasting was investigated in order to examine the impact of roasting time on the leaching efficiencies of these elements. The roasting temperature for all roasting time tests is 400 ℃, the results are shown in Fig. 5.

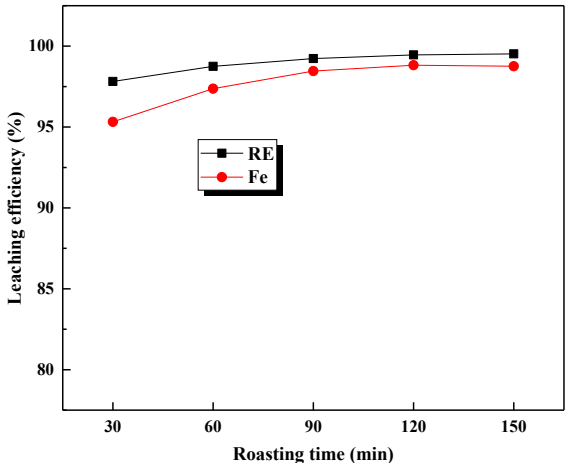

Fig. 5. Effect of roasting time on the leaching efficiencies of REEs and Fe

The leaching efficiencies of REEs and Fe are minimally affected by the roasting time, as illustrated in Fig. 5. The leaching efficiencies of REEs and Fe exhibited an upward trend as the roasting time was prolonged. When roasted at a time of 30 minutes, the REEs and Fe leaching efficiencies reached 97.82% and 95.32%, respectively. The leaching efficiencies of REEs and Fe did not exhibit a significant enhancement even upon further elevation of the roasting temperature. The generation of noticeable bubbles during the leaching process was observed when the roasting time was 30 minutes and 60 minutes.

In order to investigate the phase transition behavior of REEs and Fe for the roasted products at different roasting times, the roasted samples obtained at various time intervals were subjected to XRD analysis, and the corresponding results are presented in Figure 6. It was observed that the roasted products at 30 minutes and 60 minutes exhibited distinct metallic iron phases, indicating insufficient iron oxidation due to inadequate roasting temperature. Consequently, hydrogen gas was generated during the hydrochloric acid leaching process. The REEs and Fe phases were both oxidized when the roasting time exceeded 90 minutes, and no bubbles were observed during the leaching process. Therefore, it was determined that the optimal roasting time is 90 minutes.

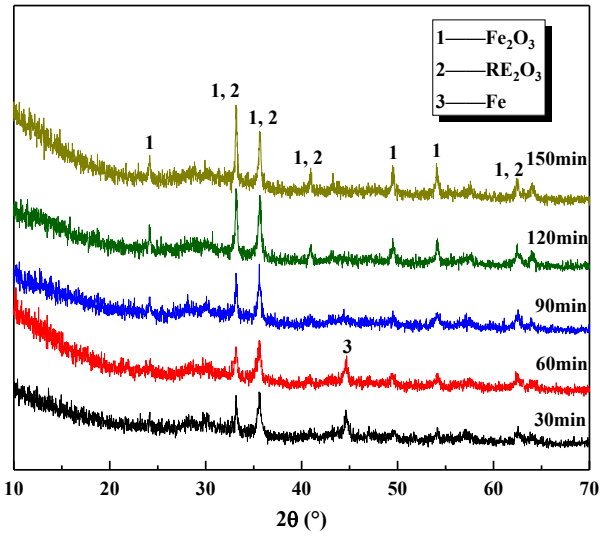

Fig. 6. XRD of roasted products for different roasting time

3.2. Leaching kinetics of REEs and Fe

The leaching rates of REEs and Fe exhibit significant disparity, as evidenced by our previous research (Liu et al., 2022). The dissolution rate of rare earth oxide is significantly higher than that of iron oxide due to its more reactive chemical properties, while the dissolution rate of iron oxide remains comparatively slower. The investigation of the co-leaching kinetics of REEs and Fe is therefore deemed necessary.

The leaching process of REEs and Fe from NdFeB waste is characterized by solid-liquid two-phase reaction, where the rate-controlling steps include chemical reaction and reactant diffusion. The shrinking core model is presently the predominant solid-liquid reaction kinetics model (Yang et al., 2023; Xue et al., 2017). The leaching process of roasted NdFeB waste can be characterized as a dissolution process of RE_2O_3 and Fe_2O_3, as evidenced by the results presented in Fig. 3 and Fig. 4. This suggests that the acid leaching kinetics of NdFeB waste closely align with the applicable conditions of the shrinkage core model. The leaching reactions of REEs and Fe are assumed to adhere to the shrinking core model.

The kinetic equation in Eq. 3 represents the control of reaction rate by a chemical reaction (Wu et al., 2023; Zhang et al., 2016).

$$k_C t = 1 - (1 - x)^{\frac{1}{3}} \tag{3}$$

The kinetic equation in Eq.4 represents the reaction rate when it is controlled by interior diffusion (Wu et al., 2023; Zhang et al., 2016).

$$k_D t = 1 - 3(1 - x)^{\frac{2}{3}} + 2(1 - x \tag{4}$$

The kinetic equation for the reaction rate, which is controlled by both mixing and chemical reactions at the interface as well as solid film diffusion, can be expressed as Eq. 5 (Wu et al., 2023; Zhang et al., 2016).

$$k_M t = \frac{1}{3} ln(1-x) - 1 + (1-x)^{-\frac{1}{3}} \quad (5)$$

where, x represents the leaching efficiency, t is the leaching time (min), k_C is the chemical reaction rate constant (min^{-1}), k_D represents the diffusion rate constant (min^{-1}), and k_M is the apparent rate constant (min^{-1}).

The leaching rate of rare earths was considerably higher than that of iron, as indicated by our previous research findings (Liu et al., 2022). The leaching efficiencies of REEs and Fe were investigated at different time intervals and temperatures in order to further elucidate the dissolution mechanism, as depicted in Fig. 7. The leaching efficiencies of REEs and Fe obtained at different temperatures and times were then substituted into Eq. 3, Eq. 4, and Eq. 5 for linear fitting. The resulting data is presented in Fig. 8, Fig. 9, and Fig. 10. The rate constant values (k_C, k_D and k_M) and correlation coefficients (R^2) obtained from the plots of chemical, diffusion and mixed controlled models are given in Table 2 and Table 3.

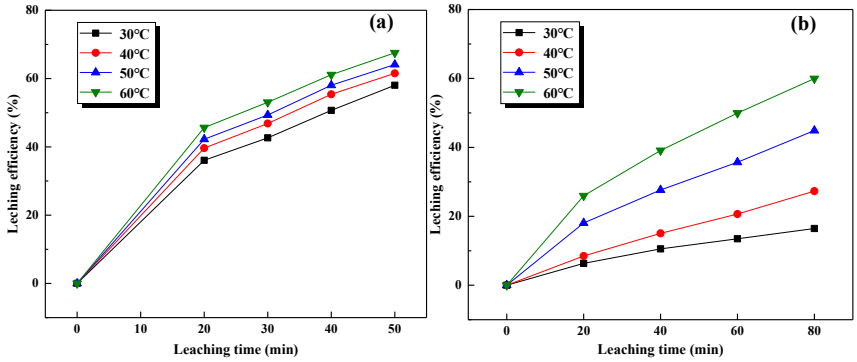

Fig. 7. Leaching efficiencies of REEs (a) and Fe (b) at different times and temperatures

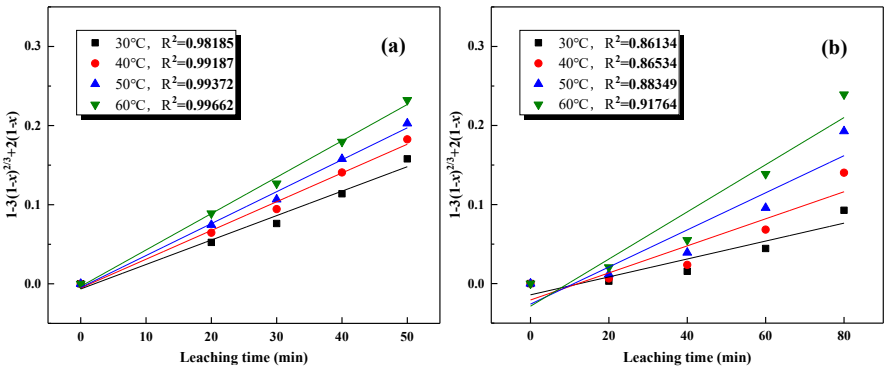

Fig. 8. Linear-fitting results of the interior diffusion control: (a) REEs, (b) Fe

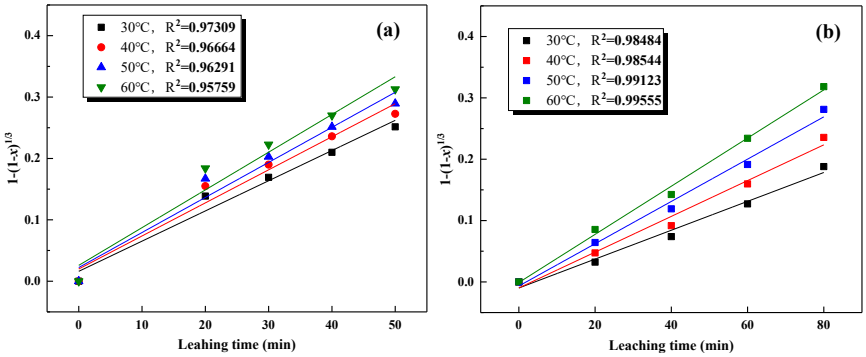

Fig. 9. Linear-fitting results of the chemical reaction control: (a) REEs, (b) Fe

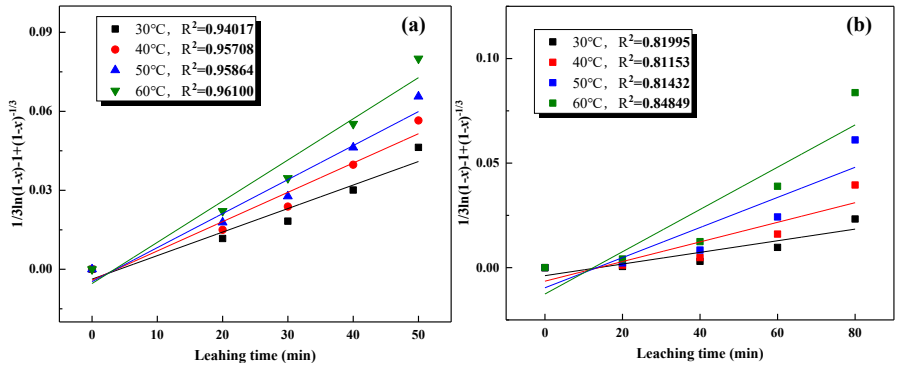

Fig. 10. Linear-fitting results of the mixed reaction control. (a) REEs, (b) Fe

Table 2. Values of apparent rate constants (k), correlation coefficient (R^2) for different leaching kinetic models of REE

Temperature (°C)	Interior diffusion control		Chemical reaction control		Mixed reaction control	
	k_D	R^2	k_C	R^2	k_M	R^2
30	0.00309	0.98185	0.00492	0.97309	0.00089	0.94017
40	0.00363	0.99187	0.00539	0.96664	0.00111	0.95708
50	0.00404	0.99372	0.00571	0.96291	0.00129	0.95864
60	0.00464	0.99327	0.00615	0.95759	0.00156	0.96100

Table 3. Values of apparent rate constants (k), correlation coefficient (R^2) for different leaching kinetic models of Fe

Temperature (°C)	Interior diffusion control		Chemical reaction control		Mixed reaction control	
	k_D	R^2	k_C	R^2	k_M	R^2
30	0.00113	0.8613	0.00118	0.9976	0.00028	0.81995
40	0.00171	0.8653	0.00202	0.9841	0.00047	0.81153
50	0.00235	0.8835	0.00358	0.9969	0.00072	0.81432
60	0.00298	0.9176	0.00527	0.9984	0.00101	0.84849

The R^2 value of the REEs fitting equation for interior diffusion control, as depicted in Fig. 7, approaches unity, indicating a high level of fit and that the fitted curve passes through the origin. The R^2 value of the iron fitting equation, however, was relatively low, indicating a suboptimal fit and a lack of alignment with the zero-intercept for the fitted curve. The above results suggested that the leaching of REEs is predominantly governed by internal diffusion.

As depicted in Fig. 8, the R^2 value of the rare earth fitting equation for chemical reaction control was relatively lower, indicating a poorer fit and a non-zero intercept for the fitting curve. The iron fitting equation exhibited a high R^2 value close to 1, indicating an excellent fit, and the fitting curve precisely intersected the origin. The preliminary findings indicated that the process of iron leaching is predominantly governed by chemical reactions.

As depicted in Fig. 9, the R^2 values for the fitting equations of REEs and Fe in the mixed reaction control were relatively low, indicating that the fitted curves do not accurately pass through the origin. The absence of a mixed reaction suggested that the REEs and Fe were not under combined control.

According to Arrhenius equation, it can be deduced the kinetics equation of leaching：

$$ln\,k = -\frac{E}{RT} + ln\,A \quad (6)$$

where, k is the apparent rate constant (min^{-1}); E is the apparent activation energy(kJ/mol); R is the ideal gas constant; T is the thermodynamic temperature(K); A is the frequency factor.

Eq. 6 indicated that ln$k$ demonstrates a linear correlation with $1/T$, and the slope corresponds to -E/R. Therefore, The apparent activation energy can be determined by calculating the slope of -E/R.。 The negative logarithm of the reaction rate constant k, obtained from Table 2 and Table 3, is plotted against the reciprocal of leaching temperature T in Fig. 11.

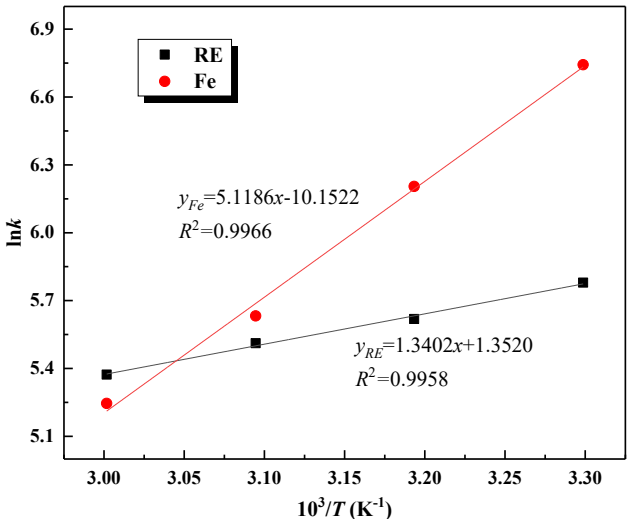

Fig. 11. Linear-fitting results of Arrhenius equation

The results presented in Fig. 10 demonstrate that the fitting curves for the ln(k) versus 1/T plots exhibit slopes of 1.3402 and 5.1186 for REEs and Fe, respectively. The apparent activation energies for REEs and Fe can be calculated as 11.14 kJ/mol and 42.56 kJ/mol, respectively, based on these findings. According to the classical kinetic theory (Zhou et al., 2022; Brahim et al., 2022), leaching reactions were governed by internal diffusion when the apparent activation energy was below 12 kJ/mol. The chemical reactions exerted control when the energy exceeded 41.8 kJ/mol, while a combination of factors influenced the control when it falled between 12 kJ/mol and 41.8 kJ/mol. The leaching of REEs during the NdFeB leaching process was primarily governed by internal diffusion, while the leaching of iron is predominantly controlled by chemical reactions.

According to Arrhenius equation theory，the rate of a chemical reaction was closely correlated with the magnitude of its activation energy, whereby a decrease in activation energy led to an acceleration in reaction rates (Xu et al., 2024). The results of our previous studies consistently demonstrate that, when leaching NdFeB waste, the leaching efficiency of REEs always surpasses that of Fe under identical conditions. The results presented in Fig. 10 indicate that the apparent activation energy of rare earth (11.14 kJ/mol) is comparatively lower than that of iron (42.56 kJ/mol). Therefore, the leaching rate of rare earth in the NdFeB waste leaching process is higher than that of iron. The leaching reaction of REE reached equilibrium before any other reactions as time progresses.

4. Conclusions

(1) The oxidation roasting of NdFeB waste involved an intricate phase transition process. The leaching rates of REEs and Fe demonstrate a gradual decrease as the oxidation roasting temperature increases, particularly for Fe, where the decline in leaching rate is more pronounced.

(2) The XRD results indicated that the REEs and Fe in the oxidized roasting product existed predominantly as RE_2O_3 and Fe_2O_3 phases. The SEM results indicated that with an increase in roasting temperature, the material surface exhibited a higher propensity for the formation of compact “spherical” structures, thereby impeding the penetration of hydrochloric acid leaching agent into the material core and consequently reducing the leaching rate of REEs and Fe. The oxidation of Ce to insoluble CeO_2 at high temperatures further diminishes the leaching rate of REEs.

(3) The co-leaching kinetics of the NdFeB waste indicated that REEs were primarily controlled by internal diffusion, while Fe was predominantly controlled by chemical reactions. The apparent activation energy for REEs was less than that of iron. Consequently, during the co-leaching process, the leaching rate of REEs from NdFeB waste exceeded that of Fe, and the leaching reaction of REE reached equilibrium before any other reactions as time progresses

Acknowledgments

This work was supported by the Open Project for Key Laboratory of Testing and Tracing of Rare Earth Products for State Market Regulation, Jiangxi University of Science and Technology (No. TTREP2022ZD01 and TTREP2022YB02).

References

PROSPERI, D., BEVAN, A. I., ROSILLO, G. U., TUDOR, C. O., FURLAN, G., DOVE, S., LUCIA, P., ZAKOTNIK, M, 2018. *Performance comparison of motors fitted with magnet-to-magnet recycled or conventionally manufactured sintered NdFeB*. J. Magn. Magn. Mater. 460, 448–453.

AMBAYE, T. G., VACCARI, M., CASTRO, F. D., PRASAD, S., RTIMI S, 2020. *Emerging technologies for the recovery of REEs (REEs) from the end-of-life electronic wastes: A review on progress, challenges, and perspectives*. Environ. Sci. Pollut. Res. 27, 36052–36074.

BRIÃO, G. V., SILVA, M. G., VIEIRA, M. G. A.,2022. *Adsorption potential for the concentration and recovery of rare earth metals from NdFeB magnet scrap in the hydrometallurgical route: A review in a circular economy approach*. J. Cleaner Prod. 380, 135112.

JYOTHI, R. K., THENEPALLI, T., AHN, J. W., PARHI, P. K., K. CHUNG, W., J. Lee, 2020. *Review of REEs recovery from secondary resources for clean energy technologies: Grand opportunities to create wealth from waste*. J. Cleaner Prod. 267, 122048.

CHEN, X., SUN, Y., WANG, L., QU, X., ZHAO, Y., XIE, H., WANG, D., YIN, H., 2023. *Electrochemically recycling degraded superalloy and valorizing CO2 in the affordable borate-modified molten electrolyte*. Tungsten. 2661-8028.

VENKATESAN, P., Z., SIETSMA, J., YANG, Y., 2018. *An environmentally friendly electro-oxidative approach to recover valuable elements from NdFeB magnet waste*. Sep. Purif. Technol. 191, 384–391.

VENKATESAN, P., HOOGERSTRAETE, T. V., HENNEBEL, T., BINNEMANS, K., SIETSMA, J., YANG Y., 2018. *Selective electrochemical extraction of REEs from NdFeB magnet waste at room temperature*. Green Chem. 20, 1065–1073.

AWAIS, C. J. M., DEGRI, L. P. M. , ZHOU, W., BRADSHAW, A., SHERIDAN, R., MANN, V., WALTON, A., 2020. *The extraction of NdFeB magnets from automotive scrap rotors using hydrogen*. J. Cleaner Prod. 277, 124058.

BEHERA, S. S., PANDA, S. K., MANDAL, D., PARHI, P. K., 2019. *Ultrasound and Microwave assisted leaching of neodymium from waste magnet using organic solvent.* Hydrometallurgy. 185, 61–70.

KUMARI, A., RAJ, R., RANDHAWA, N.S., SUSHANTA-KUMAR, S., 2021. *Energy efficient process for recovery of rare earths from spent NdFeB magnet by chlorination roasting and water leaching*. Hydrometallurgy. 201, 105581.

DU, C., MA, S., XIE, M., YANG, F., ZHAO, Z., CHEN, Y., MA, Y., 2023. *Recovery of high-value REEs from waste NdFeB by the water-soluble ammonium salt [Hbet]cl*. Sep. Purif. Technol. 308, 122946.

BELFQUEH, S., CHAPRON, S., GIUSTI, F., PELLET-ROSTAING, S., SERON, A., MENAD, N., ARRACHART, G., 2024. *Selective recovery of REEs from acetic leachate of NdFeB magnet by solvent extraction*. Sep. Purif. Technol. 339, 126701.

YANG, Q., LI, Y., LI, B., DUAN, P., REN, Z., ZHOU, Z., 2024. *Selective leaching and recovery of neodymium from NdFeB carbonyl residues*. Sep. Purif. Technol. 329, 125137.

YU, G., NI, S., GAO, Y., MO, D., ZENG, Z., SUN, X., 2024. *Recovery of rare earth metal oxides from NdFeB magnet leachate by hydrophobic deep eutectic solvent extraction, oxalate stripping and calcination*. Hydrometallurgy. 223, 106209.

BRIÃO, G. V., LOPES, C. B., TRINDADE, T., SILVA, C. M., SILVA, M. G. C., VIEIRA, M. G. A., 2024. *NdFeB magnet scrap valorization by leaching and recovery of rare earth metals by sorption on low-cost expanded clay*. J. Ind. Eng. Chem. 131, 58–568.

HE, L., XU, Q., LI, W., DONG, Q., SUN, W., 2022. *One-step separation and recovery of rare earth and iron from NdFeB slurry via phosphoric acid leaching* J. Rare Earths. 40, 338-344.

JIN, H., AFIUNY, P., DOVE, S., FURLAN, G., ZAKOTNIK, M., YIH, Y., SUTHERLAND, J., 2018. Life Cycle

Assessment of NdFeB Magnet-to-Magnet Recycling for Electric Vehicle Motors. Environ. Sci. Technol. 52, 3796–3802.

LIU, Z., ZHOU, H., LI, W., LUO, X., WANG, J., LIU, F., 2022. *Separation and coextraction of REEs and Fe from NdFeB sludge by co-leaching and stepwise precipitation*. Sep. Purif. Technol. 282, 119795.

KUMARI, A., SINHA, M. K., PRAMANIK, S. SAHU, S. K., 2018. *Recovery of rare earths from spent NdFeB magnets of wind turbine: Leaching and kinetic aspects*. Waste Manage. 75, 486–498.

BEHERA, S.S., PARHI, P.K., 2016. *Leaching kinetics study of neodymium from the scrap magnet using acetic acid*. Sep. Purif. Technol. 160, 59–66.

GENERAL ADMINISTRATION OF QUALITY SUPERVISION, Inspection and Quarantine of the People's Republic of China, Standardization Administration of the People's Republic of China., 2009.Irons—*Determination of total iron content—Titanium(III) chloride reduction potassium dichromate titration methods (routine methods)* (GB/T 6730.65-2009).

FIRDAUS, M., RHAMDHANI, M. A., RANKIN, W. J., POWNCEBY, M., WEBSTER, N.A.S., D'ANGELO, A. M., MCGREGOR, K., 2018. *High temperature oxidation of rare earth permanent magnets. Part 1 – Microstructure evolution and general mechanism*. Corros. Sci. 133, 374-385.

ZHANG, Z., WANG, D., LIU, C., ZHI, W., XIAO, W., QIAN, G., LI, G., 2022. *New insight into oxidative roasting and leaching for NdFeB waste*, J. Environ. Chem. Eng., 10(6), 108946.

YANG, H., SHA, A., HE, Z., WU, C., XU, Y., HU, J., XU, Z., RUAN, C., 2023. *Leaching kinetics and permeability of polyethyleneimine added ammonium sulfate on weathered crust elution-deposited rare earth ores*. J. Rare Earths. http://doi.org./10.1016/j.jre.2023.08.022.

XUE, N., ZHANG, Y., HUANG, J., LIU, T., WANG, L., 2017. *Separation of impurities aluminum and iron during pressure acid leaching of vanadium from stone coal*. J. Cleaner Prod. 166, 1265–1273.

WU, H., YAN, H., LIANG, Y., QIU, S., ZHOU, X., ZHU, D., QIU, T., 2023. *Rare earth recovery from fluoride molten-salt electrolytic slag by sodium carbonate roasting-hydrochloric acid leaching*. J Rare Earths. 41, 1242–1249.

ZHANG, C., MIN, X., ZHANG, J., WANG, M., LI, Y., FEI, J., 2016. *Reductive clean leaching process of cadmium from hydrometallurgical zinc neutral leaching residue using sulfur dioxide*. J. Cleaner. Prod. 113, 910–918.

ZHOU, Y., LIU, J., CHENG, G., XUE, X., YANG, H., 2022. *Kinetics and mechanism of hydrochloric acid leaching of rare earths from Bayan Obo slag and recovery of rare earth oxalate and high purity oxides*. Hydrometallurgy. 208, 105782.

BRAHIM, J. A., HAK, S. A., ACHIOU, B., BOULIF, R., BENIAZZA, R., BENHIDA, R., 2022. *Kinetics and mechanisms of leaching of REEs from secondary resources*. Miner. Eng. 177, 107351.

XU, X., JIA, X., JING, P., ZHANG, Y., CUI, J., ZUZEK, K., SASO, S., LIU, ZHANG, B., J., 2024. *In situ anodic leaching of Nd-Fe-B sludge with fast leaching kinetics for selective recovery of rare-earth elements*. J. Rare Earths. https://doi.org/10.1016/j.jre.2024.02.001.